Progressive nigrostriatal terminal dysfunction and degeneration in the engrailed1 heterozygous mouse model of Parkinson's disease

Geneviève Beauvais, Anamitra Ghosh, Baby Chakrapani Pulikkaparambil Sasidharan, Martin Lundblad, Julia Fuchs, Rajiv L Joshi, Jack Lipton, Andrew Roholt, Satish Medicetty, Timothy Feinstein, et al.

Neurobiology of Disease 73 (2015) 70–82

Contents lists available at ScienceDirect

Neurobiology of Disease

journal homepage: www.elsevier.com/locate/ynbdi

Progressive nigrostriatal terminal dysfunction and degeneration in the engrailed1 heterozygous mouse model of Parkinson's disease

Ulrika Nordström [a,1], Geneviève Beauvais [b,1], Anamitra Ghosh [b], Baby Chakrapani Pulikkaparambil Sasidharan [b], Martin Lundblad [c], Julia Fuchs [d,e,f], Rajiv L. Joshi [d,e,f], Jack W. Lipton [g,h], Andrew Roholt [i], Satish Medicetty [i], Timothy N. Feinstein [j], Jennifer A. Steiner [b], Martha L. Escobar Galvis [b], Alain Prochiantz [d,e,f], Patrik Brundin [a,b,*]

[a] Neuronal Survival Unit, Wallenberg Neuroscience Center, Department of Experimental Medical Science, Lund University, BMC B11, 221 84 Lund, Sweden
[b] Laboratory of Translational Parkinson's Disease Research, Center for Neurodegenerative Science, Van Andel Research Institute, 333 Bostwick Ave, N.E., Grand Rapids, MI 49503, USA
[c] Developmental and Regenerative Neurobiology, Wallenberg Neuroscience Center, Department of Experimental Medical Science, Lund University, BMC A11, 221 84 Lund, Sweden
[d] Collège de France, Center for Interdisciplinary Research in Biology (CIRB), Paris, France
[e] Centre National de la Recherche Scientifique, Unité Mixte de Recherche 7241, Paris, France
[f] Institut National de la Santé et de la Recherche Médicale U1050, Labex Memolife, Paris, France
[g] Department of Translational Science and Molecular Medicine, Michigan State University, Grand Rapids, MI 49503, USA
[h] The Udall Center of Excellence in Parkinson's Disease Research, Michigan State University, Grand Rapids, MI 49503, USA
[i] Renovo Neural, Inc., 10000 Cedar Avenue, Cleveland, OH 44106, USA
[j] Confocal Microscopy and Quantitative Imaging Core Facility, Van Andel Research Institute, 333 Bostwick Ave, N.E., Grand Rapids, MI 49503, USA

ARTICLE INFO

Article history:
Received 11 June 2014
Revised 28 August 2014
Accepted 21 September 2014
Available online 2 October 2014

Keywords:
Retrograde degeneration
TH–GFP
En1$^{+/-}$ mice
CLARITY
In vivo electrochemistry
Impaired dopamine release
Dopamine transporter
Autophagy
mTOR
LC3

ABSTRACT

Current research on Parkinson's disease (PD) pathogenesis requires relevant animal models that mimic the gradual and progressive development of neuronal dysfunction and degeneration that characterizes the disease. Polymorphisms in engrailed 1 (En1), a homeobox transcription factor that is crucial for both the development and survival of mesencephalic dopaminergic neurons, are associated with sporadic PD. This suggests that En1 mutant mice might be a promising candidate PD model. Indeed, a mouse that lacks one *En1* allele exhibits decreased mitochondrial complex I activity and progressive midbrain dopamine neuron degeneration in adulthood, both features associated with PD. We aimed to further characterize the disease-like phenotype of these *En1*$^{+/-}$ mice with a focus on early neurodegenerative changes that can be utilized to score efficacy of future disease modifying studies. We observed early terminal defects in the dopaminergic nigrostriatal pathway in *En1*$^{+/-}$ mice. Several weeks before a significant loss of dopaminergic neurons in the substantia nigra could be detected, we found that striatal terminals expressing high levels of dopaminergic neuron markers TH, VMAT2, and DAT were dystrophic and swollen. Using transmission electron microscopy, we identified electron dense bodies consistent with abnormal autophagic vacuoles in these terminal swellings. In line with these findings, we detected an up-regulation of the mTOR pathway, concurrent with a downregulation of the autophagic marker LC3B, in ventral midbrain and nigral dopaminergic neurons of the *En1*$^{+/-}$ mice. This supports the notion that autophagic protein degradation is reduced in the absence of one *En1* allele. We imaged the nigrostriatal pathway using the CLARITY technique and observed many fragmented axons in the medial forebrain bundle of the *En1*$^{+/-}$ mice, consistent with axonal maintenance failure. Using in vivo electrochemistry, we found that nigrostriatal terminals in the dorsal striatum were severely deficient in dopamine release and reuptake. Our findings support a progressive retrograde degeneration of *En1*$^{+/-}$ nigrostriatal neurons, akin to what is suggested to occur in PD. We suggest that using the *En1*$^{+/-}$ mice as a model will provide further key insights into PD pathogenesis, and propose that axon terminal integrity and function can be utilized to estimate dopaminergic neuron health and efficacy of experimental PD therapies.

Introduction

Parkinson's disease (PD) is a progressive neurodegenerative disorder affecting multiple neuronal systems. Mitochondrial dysfunction, altered autophagy, and aggregation of α-synuclein are among the pathogenic events suggested to play key roles in the disorder (Sanchez-Perez et al.,

* Corresponding author at: Van Andel Institute |www.vai.org, 333 Bostwick Ave. N.E., Grand Rapids, Michigan 49503-2518, USA. Fax: +1 616 234 5129.
E-mail address: Patrik.Brundin@vai.org (P. Brundin).
Available online on ScienceDirect (www.sciencedirect.com).
[1] These authors contributed equally.

http://dx.doi.org/10.1016/j.nbd.2014.09.012
0969-9961/

2012; Schapira, 2011). Failure of nigrostriatal dopamine neurotransmission and degeneration of dopaminergic neurons in the substantia nigra are particularly prominent in PD and are believed to underlie the classic motor dysfunctions. Recent studies of patient autopsy material have suggested that the disease process is initiated at the level of the dopamine terminals in the striatum and that the neuronal death, i.e. loss of cell bodies in the substantia nigra occurs later (Burke and O'Malley, 2013; Kordower et al, 2013). Several rodent PD models have been used to explore different aspects of dopamine neuron degeneration (Bezard et al., 2013; Blesa et al., 2012). Chiefly among them are the toxin-based models, e.g. injections of 1-methyl-4-phenyl-1,2,3,6-tetrahydropyridine (MPTP) or 6-hydroxydopamine (6-OHDA), which cause failure of mitochondrial respiration and relatively rapid death of the dopaminergic neurons (Bezard et al., 2013). However, these models do not faithfully recreate the protracted degeneration of dopaminergic neurons suggested to occur in PD, which seems to start in the dopaminergic striatal terminals and culminate in the death of nigral neurons months to years later. We expect the models that mimic these features to be more relevant to PD.

Recent genetic analyses have implicated a human gene called engrailed1 (*En1*) in the pathogenesis of PD, reporting that a polymorphism of *En1* might tentatively be associated with increased PD susceptibility (Fuchs et al., 2009). The *En1* gene encodes a protein expressed both in developing and mature dopaminergic neurons (Le Pen et al., 2008; Sonnier et al., 2007). En1 is also involved in axon guidance (Brunet et al., 2005; Wizenmann et al., 2009), and controls axonal maintenance by regulating axonal translation, axonal transport, and mitochondrial function in the axon of retinal ganglion cells (Yoon et al., 2012). Deletion of the *En1* gene in mice causes specific changes in the midbrain dopaminergic neurons. Homozygous deletion of the gene ($En1^{-/-}$) can result in total perinatal loss of dopaminergic neurons, various developmental defects, and death at birth (Wurst et al., 1994). Unlike $En1^{-/-}$ mice, animals lacking one *En1* allele ($En1^{+/-}$) are viable and born with a normal number of dopaminergic neurons in the substantia nigra. But within 6 weeks after birth, the $En1^{+/-}$ mice exhibit early signs of substantia nigra dopamine neuron degeneration. This is coupled with the depletion of striatal dopamine and motor dysfunction, which take months to fully develop (Sonnier et al., 2007). Furthermore, there is a decreased activity of the mitochondrial complex I in $En1^{+/-}$ dopaminergic neurons (Alvarez-Fischer et al., 2011). Infusion of En1 protein protects the dopaminergic neurons against mitochondrial toxins by enhancing the translation of mitochondrial complex I proteins (Alvarez-Fischer et al., 2011). In sum, the $En1^{+/-}$ mouse model recapitulates the key features of the slow progressive human PD pathogenesis, and is therefore an interesting model in which to evaluate the potential disease-modifying therapies. In the present study, we aimed to further characterize the neurodegenerative events in $En1^{+/-}$ mice with a focus on early changes that can be utilized to score efficacy when evaluating experimental therapies. Here we report that $En1^{+/-}$ dopaminergic neurons display axono-pathology several weeks to months before dopaminergic neuron death occurs, and that defective autophagy is likely to play a role in the degenerative process.

Results

Progressive degeneration of dopaminergic neurons in $En1^{+/-}$ mice

We first set out to validate our transgenic mouse lines by analyzing the proper localization of dopamine neuronal markers. Mice heterozygous for *En1* expressed the knock-in gene *LacZ* in the *En1* locus. Thus, we used expression of the β-galactosidase (β-gal) protein as a reporter for En1-lacking cells in the $En1^{+/-}$ mutant mice. We found that the *En1* locus was still active in adult mice, resulting in β-gal protein expression in the nigral tyrosine hydroxylase (TH)-positive dopaminergic neurons of the $En1^{+/-}$ mice. The wild-type (WT) mice, in contrast, did not express β-gal (Fig. 1A). We also used immunohistochemistry with an antibody that recognizes En1 (and its homolog En2), to confirm that En proteins were expressed in nigral dopaminergic neurons during adulthood (Fig. 1B). We used a double mutant dopamine neuron reporter line to facilitate monitoring of dopamine cell morphology and integrity by crossing WT and $En1^{+/-}$ mice to a reporter mouse expressing green fluorescent protein (GFP) under control of the *TH* promoter (Sawamoto et al., 2001). As expected, the majority of TH-positive cells in the midbrain expressed GFP in these mice (Fig. 1C).

To evaluate the effect of *En1* knockdown on the survival of midbrain dopaminergic neurons, we performed stereological counts of TH-immunopositive neurons in the substantia nigra of $En1^{+/-}$ and control WT littermates at various ages (4, 16, and 24 weeks) (Fig. 2A). In agreement with a previous report (Sonnier et al., 2007), we observed no difference in the number of TH-positive nigral neurons between the groups at 4 weeks, but the number of TH neurons was significantly reduced in the $En1^{+/-}$ mice at 16 weeks (18%) and 24 weeks (40%) (Fig. 2B). To test whether loss of TH neuron number progressively increased with age, we performed a two-factor ANOVA analysis that revealed significant genotype ($F(1,36) = 62.03$, $p < 0.0001$), age ($F(2,36) = 15.90$, $p < 0.0001$) and interaction effects ($F(2,36) = 24.22$, $p < 0.0001$). Additionally, the TH level in individually-sampled dopaminergic neurons was not different between the WT and $En1^{+/-}$ mice (data not shown, Student's *t*-test, $p > 0.05$) at 4 weeks of age, indicating that TH downregulation is not evident at this young age. These results demonstrate that the $En1^{+/-}$ mice are born with a normal number of dopaminergic neurons, and display an age-dependent, slow, progressive loss of TH-positive cells in the substantia nigra.

Progressive reduction of markers of dopamine neuron function in the nigrostriatal pathway of $En1^{+/-}$ mice

We performed an immunoblot analysis on midbrain tissues to monitor if TH protein levels mirrored the progressive loss of TH-positive neurons. We found that the TH levels in the $En1^{+/-}$ mice at 4, 16, and 24 weeks of age were 17–44% lower than those of the WT mice (Fig. 2D). A two-factor ANOVA analysis revealed significant genotype ($F(1,30) = 116.5$, $p < 0.0001$) and age ($F(2, 30) = 7.448$, $p = 0.0024$) effects, as well as genotype by age interaction ($F(2,30) = 6.874$, $p = 0.0035$). Tukey's pairwise comparisons revealed significant differences between $En1^{+/-}$ 4 week- and 16 week-groups ($p < 0.05$), $En1^{+/-}$ 4 week- and 24 week-groups ($p < 0.001$), but not the $En1^{+/-}$ 16 week- and 24 week-groups. Consistent with this decline, we found that TH was reduced by 19–26% in the striatum at the same ages (Figs. 3B and C). ANOVA results indicated no age effect ($F(1, 31) = 1.12$, $p = 0.3392$) on striatal TH levels in $En1^{+/-}$ mice. We also assayed the levels of dopamine transporter (DAT) in the striatum by immunoblotting and found that DAT was 22–50% lower in the $En1^{+/-}$ mice at those ages (Figs. 3B and D). A two-factor ANOVA revealed a main effect of genotype, indicating that DAT is decreased in the $En1^{+/-}$ mice (Fig. 3D). We then used HPLC to analyze striatal levels of dopamine and its metabolite 3,4-dihydroxyphenylacetic acid (DOPAC), specifically in the caudate and putamen region (Fig. 3A). At 4 weeks of age, the dopamine level in the striatum of the $En1^{+/-}$ mice was 27% lower than that in WT controls, and it was 46% lower by 24 weeks (Fig. 3E). The levels of DOPAC in the $En1^{+/-}$ mice were not significantly different from those \of controls at 4 weeks of age, but by 24 weeks they were reduced by 39% (Fig. 3F). The ratio between the levels of dopamine and DOPAC showed an increase of 1.45-fold in the striatum of 4-week-old $En1^{+/-}$ mice relative to WT animals, indicating an increase in dopamine turnover, but there was no difference between the 24-week-old $En1^{+/-}$ and WT mice (Fig. 3G).

Early signs of nigrostriatal dopaminergic degeneration in axon terminals in the $En1^{+/-}$ mice

As described above, we found no reduction in the number of TH-immunoreactive nigral neurons in the $En1^{+/-}$ mice at 4 weeks of age,

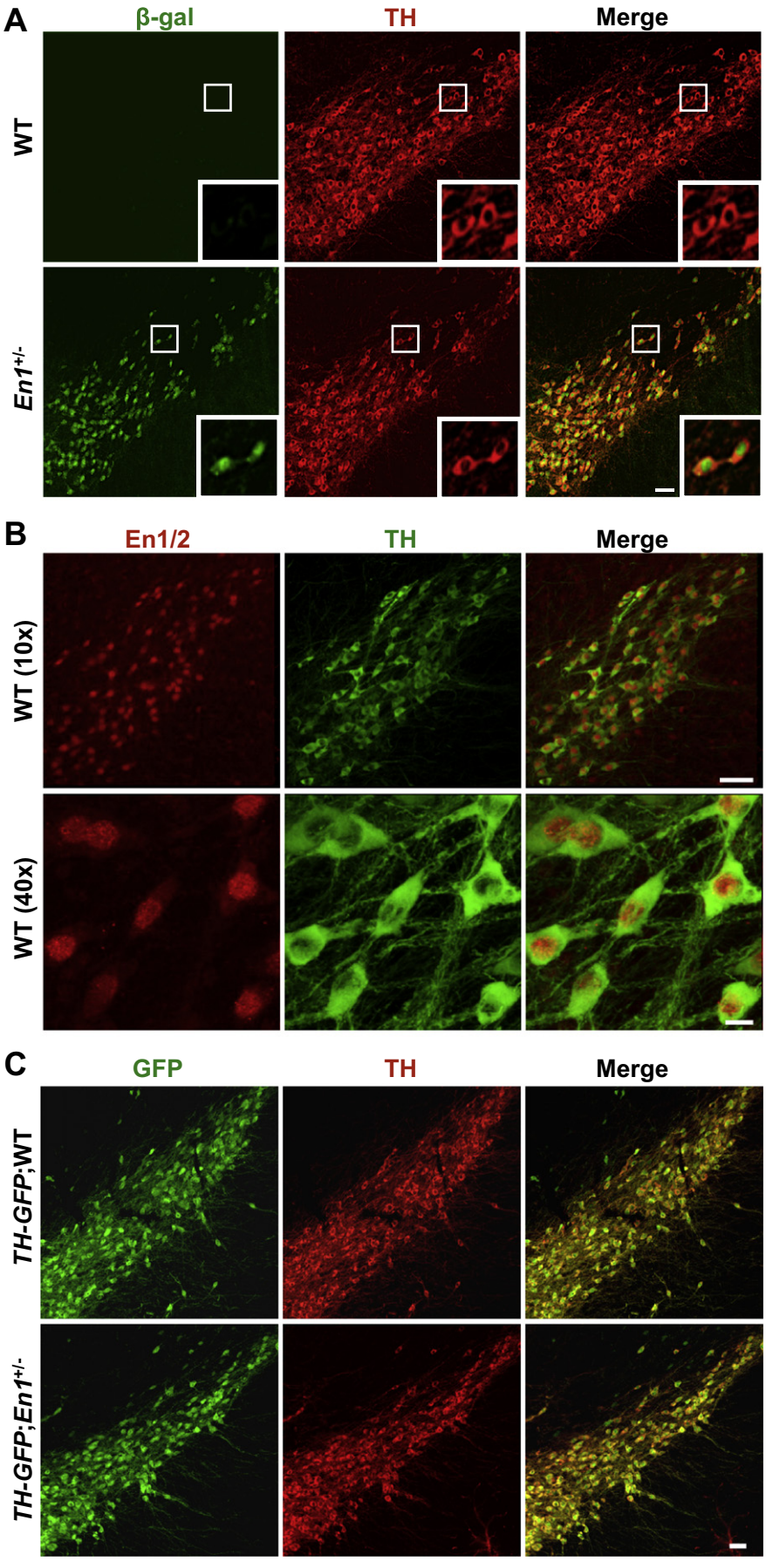
A
β-gal
TH
Merge
WT
En1+/-
B
En1/2
TH
Merge
WT (10x)
WT (40x)
C
GFP
TH
Merge
TH-GFP;WT
TH-GFP;En1+/-

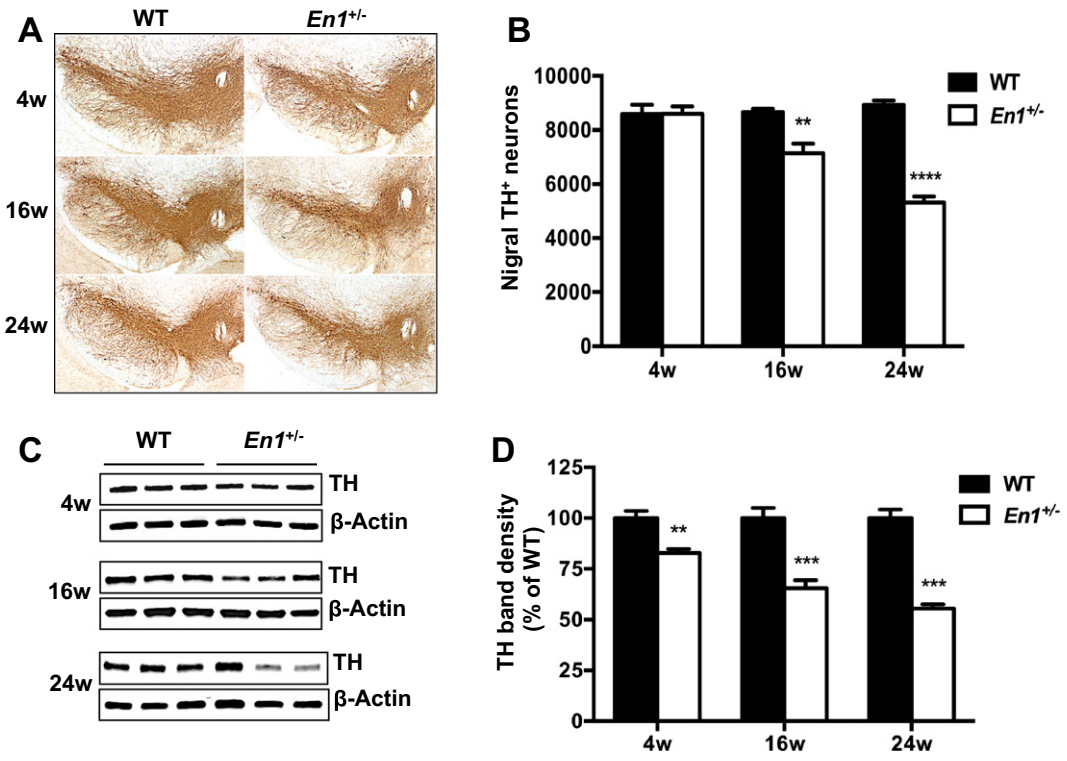

Fig. 2. Progressive loss of TH expression in the ventral midbrain of $En1^{+/-}$ mice. TH expression in the midbrain of 4-, 16-, and 24-week-old $En1^{+/-}$ and WT mice was analyzed by immunohistochemistry (A), stereology (B), and immunoblotting (C, D). A, Representative images of DAB TH staining of substantia nigra, in brain sections used to perform stereological cell counts. B, Stereological estimation of the number of TH-positive cells in the substantia nigra. Data represent means ± SEM for each group ($n = 7$ at 4 weeks; $n = 6$–7 for 16 weeks; $n = 7$–8 for 24 weeks). C, TH levels in ventral midbrain lysates were analyzed by SDS-PAGE and immunoblotting was performed in duplicate ($n = 6$ per group). β-Actin was used as an internal loading control. Representative images show three independent WT and $En1^{+/-}$ samples. D, Graph represents mean ± SEM ratios of TH band density to β-Actin. Two-factor ANOVA revealed age and genotype effects and showed that the level of intracellular TH progressively decreased in midbrain region of 4-week-, 16-week- and 24-week-old $En1^{+/-}$ mice relative to WT mice (**$p < 0.01$; ***$p < 0.001$).

but TH and dopamine were all decreased in the $En1^{+/-}$ striatum by this time. This led us to consider the possibility that the degeneration of nigrostriatal neurons begins at the level of the striatal terminals in the $En1^{+/-}$ mice. Thus, we fluorescently labeled sections through the striatum of the $En1^{+/-}$ mice and *TH–GFP*;$En1^{+/-}$ mice and monitored striatal dopamine axon terminals in confocal stacks. In striatum sections from these mice we found abnormal TH and GFP co-labeled profiles that appeared to be spheroidal dystrophic terminals of nigrostriatal neurons. We did not observe such spheroids in WT mice (Fig. 4A). The axonal spheroids were also immunoreactive for vesicular monoamine transporter 2 (VMAT2) and DAT (Figs. 4B–D). This suggests that the dystrophic terminals belong to dopamine neurons that still are capable of expressing two key proteins known to eventually be depleted in degenerating dopaminergic neurons (Kordower et al., 2013). We did not detect the spheroids in the striatum of the $En1^{+/-}$ mice at postnatal day 3. A few spheroids could be detected as early as postnatal day 8 and our quantitative analysis revealed that the density of abnormal spheroids in the striatum progressively increased from 8 days, through 4 weeks and to 24 weeks of age (A two-factor ANOVA analysis revealed significant genotype ($F(1,23) = 4327$, $P < 0.0001$) and age ($F(2,23) = 216.4$, $P < 0.0001$) effects, as well as genotype by age interaction $F(2,23) = 924$, $P < 0.0001$) (Fig. 4E). To gain further insight into the nature of the dystrophic $En1^{+/-}$ striatal terminals, we performed ultrastructural analysis on 1 mm^3 blocks of dorsal striatum from the 8-week-old mice. We observed enlarged axonal profiles displaying accumulations of mitochondria and electron-dense vacuoles in the $En1^{+/-}$ mice (Figs. 4F–G), suggesting a disturbed autophagic process. We did not observe such axonal profiles in electron micrographs from WT mice. In one $En1^{+/-}$ mouse, we measured the volume of 23 enlarged axonal profiles, which ranged from 1 μm^3 to 92 μm^3 (mean ± SEM = 25.2 ± 5.2 μm^3), which is 2–200 times the size of a normal nigrostriatal dopamine neuron terminal (Pickel et al., 1981). We hypothesized that these large axonal spheroids are indicative of axonal degeneration. To further investigate an ongoing dopamine axonal degeneration in the nigrostriatal pathway of the $En1^{+/-}$ mice, we monitored dopamine axonal integrity in the median forebrain bundle in sagittal sections through 8-week-old brains. Indeed, we found that the TH-immunoreactive axons in the median forebrain bundle were frequently swollen and appeared fragmented (Fig. 4H). By applying the CLARITY technique on 1 mm-thick brain sagittal sections, we obtained a three-dimensional view of the pathological TH-positive fibers in the median forebrain bundle of 32-week-old WT and $En1^{+/-}$ mice. We observed numerous swollen and fragmented axons in the mutant mice (Fig. 4I and Supplementary videos 1–2), indicating ongoing axonal degeneration in the nigrostriatal pathway.

Fig. 1. En1 expression in adult TH-positive dopaminergic neurons in the substantia nigra. A, Images display substantia nigra of 8-week-old WT and $En1^{LacZ}$ ($En1^{+/-}$) mice processed for TH and β-gal immunostaining. Analysis revealed expression of β-gal in the nigral TH-positive cells in *En1* heterozygote mice in which the *LacZ* gene was introduced into one *En1* allele. Analysis revealed β-gal in the majority of TH-positive cells in the substantia nigra. B, Double labeling of TH and En1/2 in 5-month-old WT mice confirmed the expression of En in adult dopaminergic neurons and showed that En proteins are mainly located to nucleus in TH-positive cells. C, Validation of the Swiss OF1 WT;*TH–GFP* and $En1^{+/-}$; *TH–GFP* mouse lines. Native GFP is visualized in sections immunolabeled for TH. The GFP is expressed under the control of the *TH* promoter and is present in the majority of the TH-positive neurons of the substantia nigra. Scale bars: A, B (10×), and C, 50 μm. Scale bar B (40×), 10 μm.

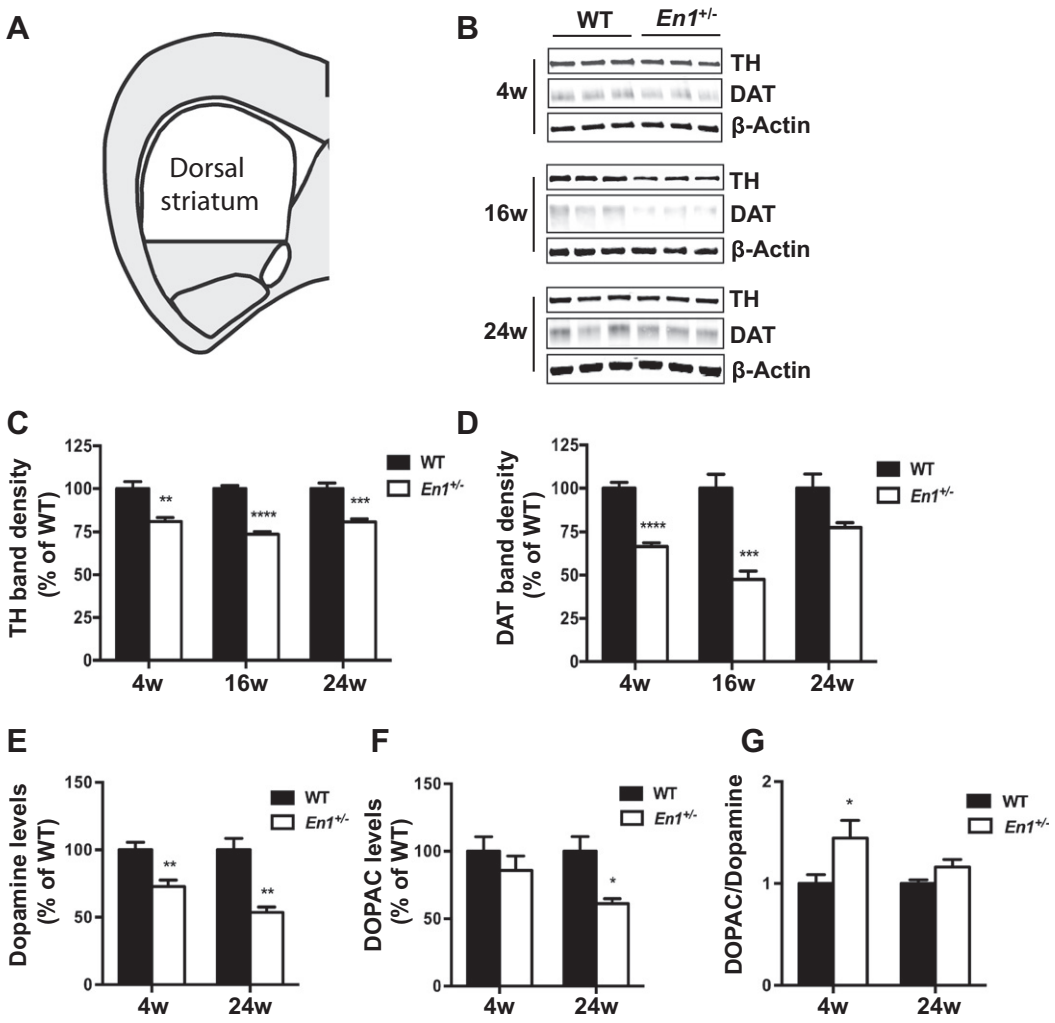

Fig. 3. Gradual loss of TH and DAT in the striatum of *En1*$^{+/-}$ mice. A, Drawing depicts the dorsal striatum containing the caudate and putamen regions dissected, and used for immunoblotting and HPLC analysis. B, The TH, DAT, and β-Actin protein levels were monitored in lysates prepared from striata of 4-week, 16-week, and 24-week-old *En1*$^{+/-}$ and WT mice. The image shows three independent striata homogenate samples per group. C, D, The TH and DAT bands on immunoblots were quantified ($n = 6$ individual samples per group), normalized to β-Actin and presented as percentages of mean ± SEM. C, The TH levels were significantly reduced in all *En1*$^{+/-}$ mice (**$p < 0.01$; ***$p < 0.001$; ****$p < 0.0001$). D, The DAT protein level was also reduced in the *En1*$^{+/-}$ samples at all ages. E, Dopamine content in the striatum (caudate and putamen regions) of 4- and 24-week-old WT and *En1*$^{+/-}$ mice as measured by HPLC and presented as percentage of WT values. Significant decreases in dopamine levels in *En1*$^{+/-}$ groups were validated by Student's *t*-test (**$p < 0.01$). F, HPLC data for DOPAC levels; significant decreases are marked (*$p < 0.05$). G, Ratio of DOPAC to dopamine (values normalized to WT) and significant increase is shown (*$p < 0.05$).

Up-regulation of the mTOR signaling pathway and reduction in the autophagic marker LC3B in the En1$^{+/-}$ *mice*

Autophagy and mTOR-regulated autophagy pathways have been implicated in numerous models of neurodegeneration (Pan et al., 2008; Son et al., 2012; Yamamoto and Yue, 2014). After observing an accumulation of numerous electron-dense autophagic vacuoles in the terminal spheroids, we hypothesized a possible alteration of mTOR signaling in the *En1*$^{+/-}$ dopamine neurons. We analyzed protein levels of mTOR signaling markers in the ventral midbrain of 16-week-old WT and the *En1*$^{+/-}$ mice by immunoblot. We found no difference in mTOR protein levels (Fig. 5A), but we observed a 2-fold increase in the nigral levels of phosphorylated (Ser 2448) mTOR (pmTOR) in the *En1*$^{+/-}$ mice (Figs. 5A and B). PmTOR, in turn, activates p70 S6 kinase. To monitor pmTOR and pS6 levels specifically in the substantia nigra, we performed immunohistochemistry and densitometric analyses. As expected, we found that pmTOR and pS6 levels were increased in the substantia nigra of the 16-week-old *En1*$^{+/-}$ mice (Figs. 5C and G). Consistent also with the upregulation of pmTOR, we observed increased (1.6-fold) phosphorylation (Ser 235/236) of S6, a downstream effector of the mTOR pathway (Figs. 5E and F). In contrast, the total S6 level of the *En1*$^{+/-}$ mice was not altered as compared to WT mice (Fig. 5E). Double-immunohistochemical labeling for TH and pmTOR revealed an accumulation of pmTOR in nigral dopaminergic neurons in the *En1*$^{+/-}$ mice (Figs. 5C and D). Similarly, we observed increased expression of pS6 in caudal midbrain sections of the *En1*$^{+/-}$ mice (Fig. 5G and H). Taken together, these results suggest that the activation of mTOR signaling pathway is upregulated in nigral dopaminergic neurons of the *En1*$^{+/-}$ mice, implying that alterations in the mTOR-mediated regulation of autophagy might be involved in the degeneration of dopaminergic neurons. In order to determine whether the absence of one *En1* allele also affected the expression of autophagic markers in the midbrain, we measured levels of the microtubule-associated protein light chain 3 (LC3B) by immunoblots on protein extracts from ventral midbrain of the 16-week-old-mice (Fig. 5I). We found a reduction in both forms of the protein, LC3B-I and LC3B-II, with a significant decrease in LC3B-II/LC3-I ratio in midbrain of the *En1*$^{+/-}$ mice, indicative of a reduction in autophagosome formation (Fig. 5J). To monitor the presence of autophagosomes in dopaminergic neurons, we performed immunofluorescence co-labeling of LC3B and TH on 16 week WT and the *En1*$^{+/-}$

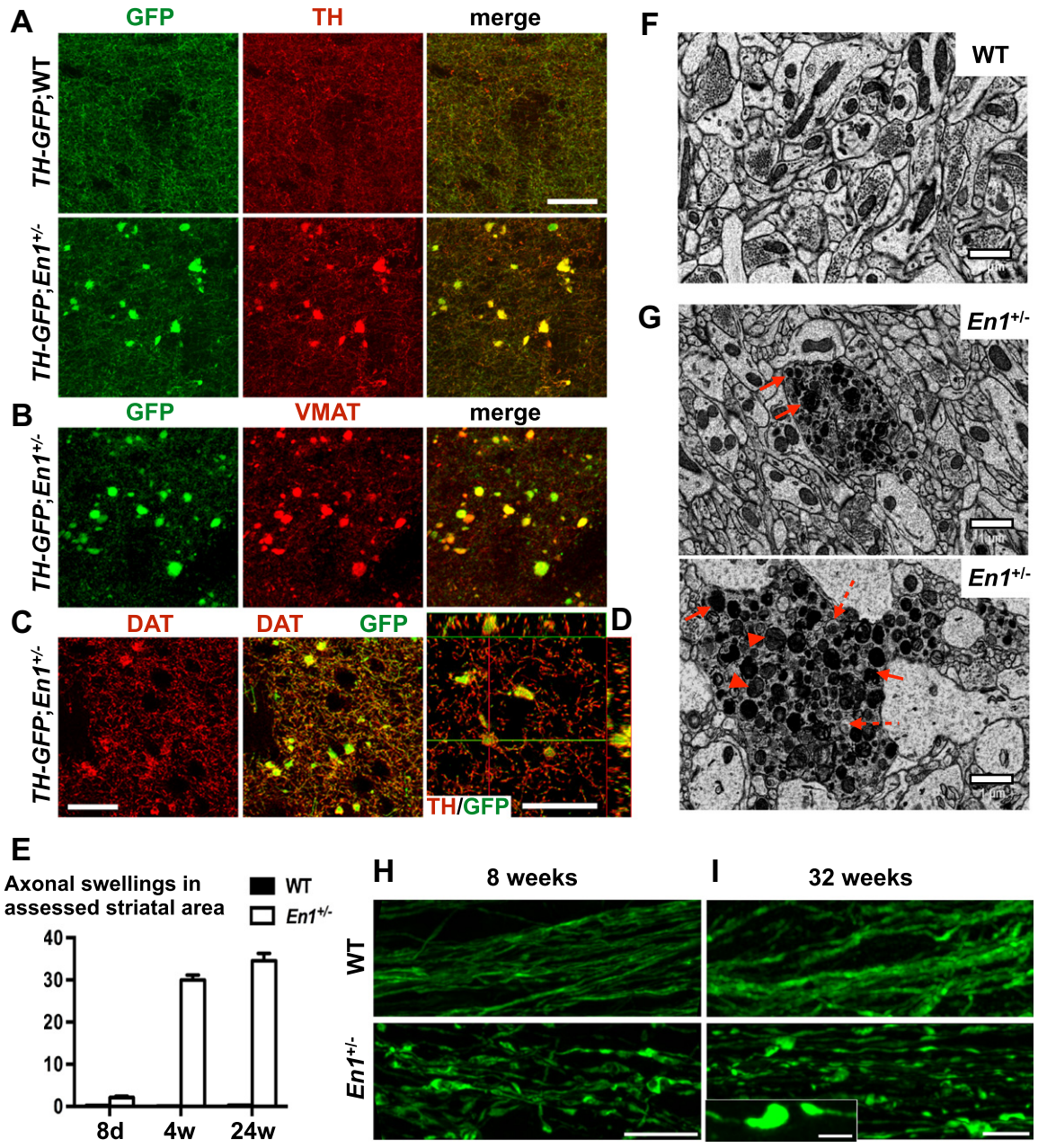

Fig. 4. Progressive distal degeneration of dopaminergic axons in *En1*$^{+/-}$ mice. A-B, Density of dopaminergic fibers shown in max projection of 6 μm confocal stacks of immunolabeled striatal sections from 8-week-old *TH–GFP*; *En1*$^{+/-}$ and *TH–GFP*; WT mice. *TH–GFP*; *En1*$^{+/-}$ mice display swollen dystrophic dopaminergic axon terminals that co-express (A) TH and GFP, (B) VMAT2 and GFP, and (C) DAT and GFP. D, Orthogonal slice view of striatal section, immunolabeled with DAT and TH, from a 16-week *En1*$^{+/-}$ animal. DAT is located in the membrane of the swollen terminal, whereas TH is located in the axoplasm. Scale bars A–D: 20 μm. E, Quantification of the swollen TH-positive terminals of 8-day-, 4-week-, and 24-week-old *En1*$^{+/-}$ mice revealed an increasing number with age ($n = 4$–5 animals/stage). F, G, TEM imaging of dorsal striatum from 8-week-old WT and *En1*$^{+/-}$ mice. F, Representative image of a WT control showing normal dendrites and synaptic components in the dorsal striatum. G, Image display abnormal enlarged axonal processes of various sizes in the striatum of *En1*$^{+/-}$ mice. These axons accumulate electron-dense bodies (arrows), abnormal autophagolysosomes (dashed arrows) and abnormal mitochondria (arrowheads). Scale bar: 1 μm. H, TH-positive fibers in the MFB region of 8-week-old *En1*$^{+/-}$ mice show disorganized and fragmented morphology, unlike those in the WT mice. Scale bar: 20 μm. I, TH-positive axonal fibers in 32-week-old *En1*$^{+/-}$ mouse brain prepared by the CLARITY technique, show discontinuous structures, not seen in WT animals. Inset shows distinct breakage site along the axon. Scale bars: 20 μm; inset scale bar: 5 μm.

midbrain sections (Fig. 5K). Quantification of the intensity of LC3B fluorescence and the number of LC3B-immunoreactive punctae present inside the nigral TH-positive neurons revealed that LC3B levels were reduced in dopaminergic neurons in the *En1*$^{+/-}$ mice (Figs. 5L, M).

Impaired striatal dopamine neurotransmission in the En1$^{+/-}$ *mice*

In light of the changes in dopamine neuron markers in the striatum of the young *En1*$^{+/-}$ mice and the early degeneration of nigrostriatal terminals, we hypothesized that nigrostriatal pathway function is impaired prior to the loss of nigral dopaminergic neurons. To test this hypothesis, we used in vivo chronoamperometric recordings of dopamine release and reuptake in the striatum of the WT and *En1*$^{+/-}$ mice. Using an assembly of a carbon fiber for dopamine detection and a glass capillary for local KCl administration, we measured dopamine release and reuptake at six different positions (separated by 250 or 500 μm) along a tract running from the dorsal to the ventral striatum (Fig. 6A, left panel). We found that the KCl-induced dopamine release (Fig. 6B) and the subsequent dopamine reuptake (Fig. 6C) were similar in the 4-week-old WT and *En1*$^{+/-}$ mice. In contrast, the 16-week-old

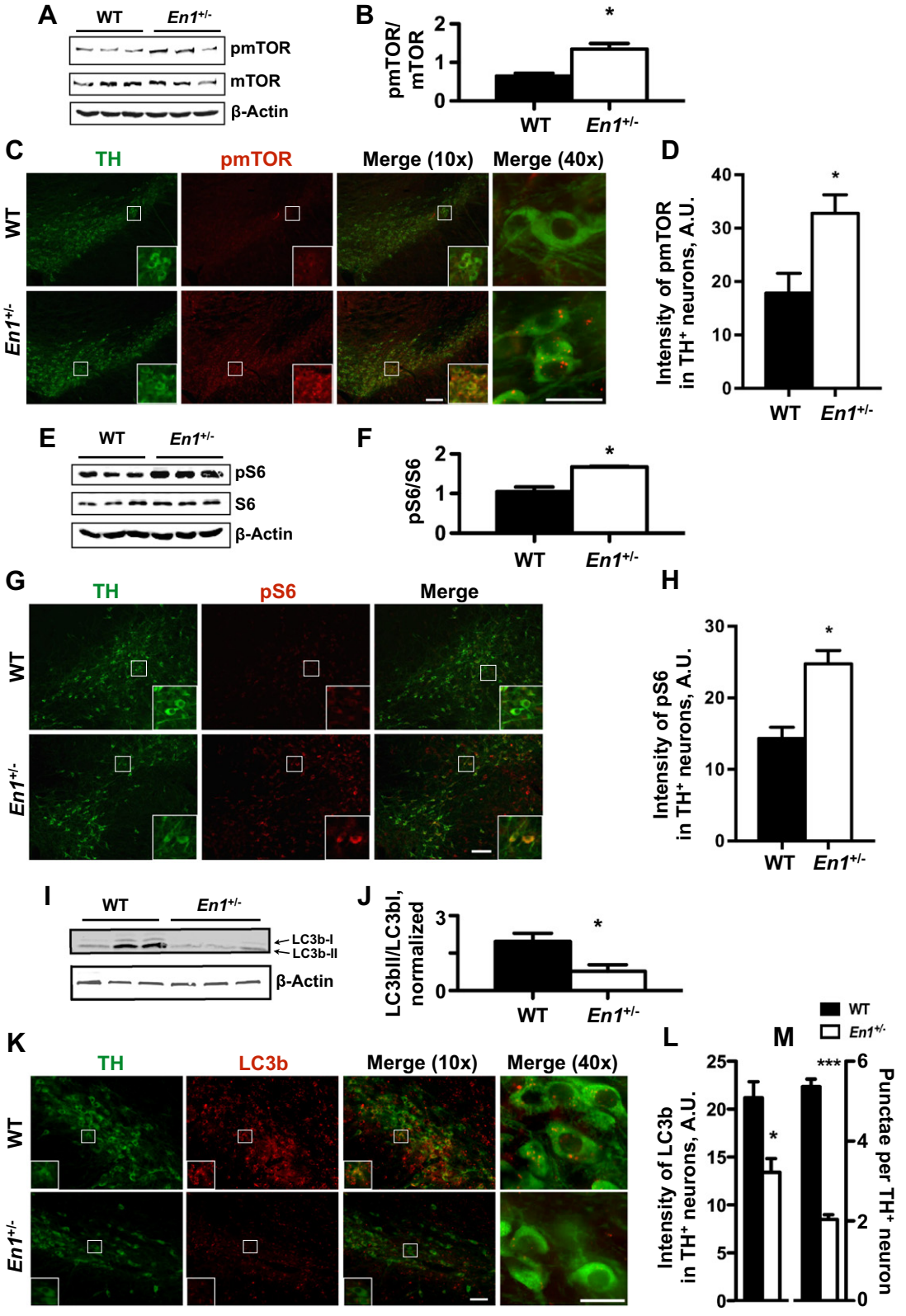

Fig. 5. Increased mTOR activation and reduction of autophagosome marker LC3II in ventral mesencephalon of *En1*$^{+/-}$ mice. A, Protein extracts from 16-week-old WT and *En1*$^{+/-}$ mice were analyzed by immunoblot for total mTOR and pmTOR in the ventral midbrain ($n = 3$ per group). Each lane represents independent samples. B, Densitometric analysis of pmTOR normalized to total mTOR. C, Substantia nigra sections of 16-week-old WT and *En1*$^{+/-}$ mice immunostained for TH and pmTOR. Inset pictures demonstrate overlap of signal of TH and pmTOR. Scale bar: 50 μm (10×) and 20 μm (40×). D, pS6 staining in the TH-positive cells (arbitrary units). E, Total S6 and pS6 proteins in the ventral midbrain ($n = 3$ per group). Each lane represents independent samples. F, pS6 densitometry normalized to total S6. Results are mean ± SEM from three mice per group. G, Substantia nigra sections of 16-week-old WT and *En1*$^{+/-}$ mice immunostained for TH and pS6. Inset pictures demonstrate overlap of signal of TH and pS6. Scale bar: 50 μm. H, pS6 staining in the TH-positive cells (arbitrary units). I-J, immunoblot analysis of LC3B-I and LC3B-II levels in lysates from 16-week-old WT and *En1*$^{+/-}$ substantia nigra, $^{*}p < 0.05$, $n = 3$ for WT and *En1*$^{+/-}$ groups. K, Images of substantia nigra regions of 16-week WT and *En1*$^{+/-}$ mice that have been fluorescently colabeled for TH and LC3B. Scale bar, 50 μm (10×) and 20 μm (40×). L, Quantification of the LC3B signal in TH-positive neurons in the substantia nigra, $^{*}p < 0.05$, $n = 3$ per group. M, Quantification of distinct LC3B-labeled punctae in TH-positive neurons in the substantia nigra, $^{***}p < 0.001$, $n = 3$ per group.

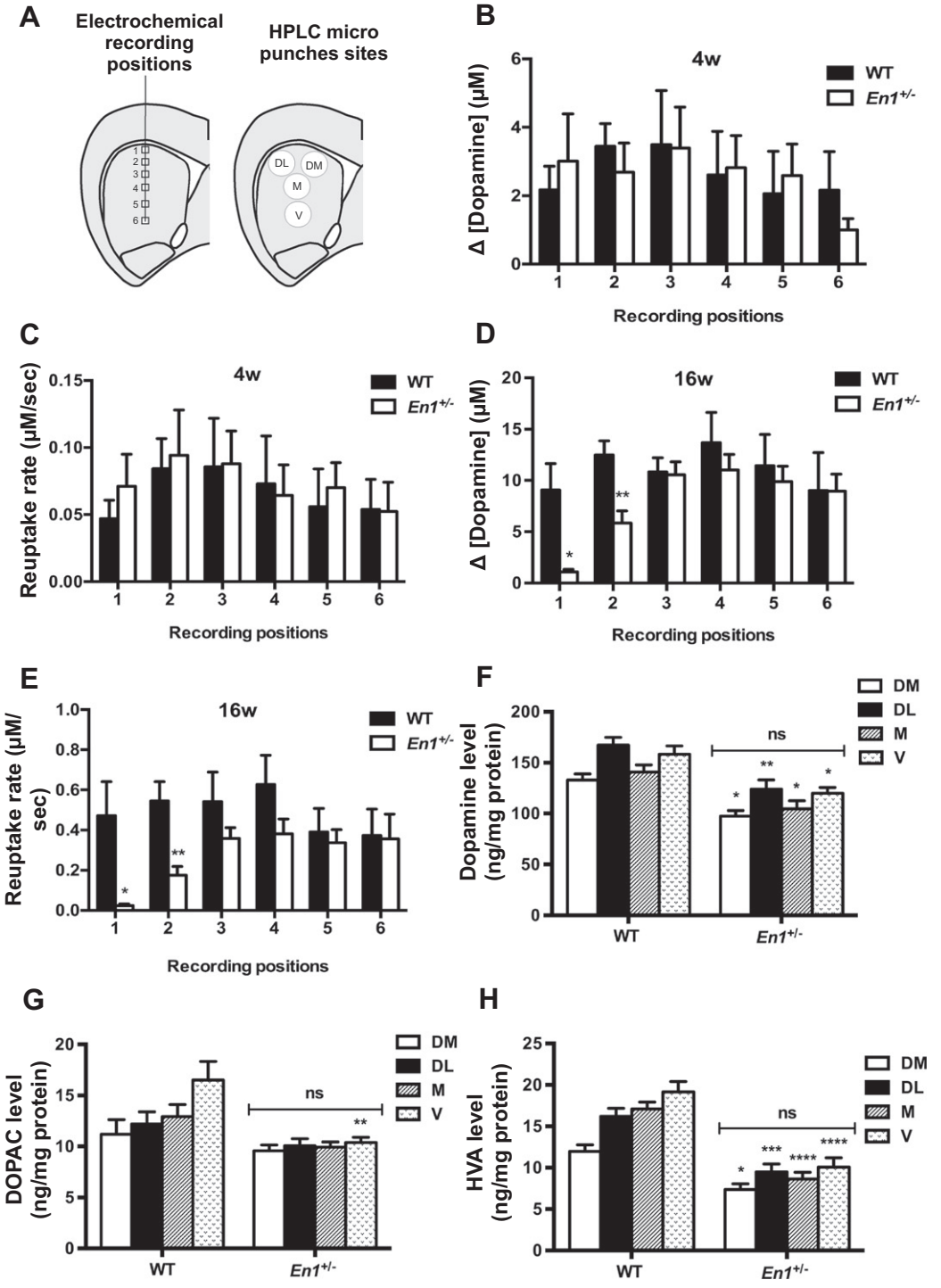

Fig. 6. $En1^{+/-}$ mice have reduced dopamine neurotransmission in the striatum. A, Left: Schematic image of striatal electrode insertion site, and positions 1–6 where KCl was injected and the in vivo electrochemical recordings were done. Right: Circles represent the subregions of the striatum where punches were taken for HPLC analysis. B and D, graphs represent means ± SEM values for estimated dopamine release in response to KCl stimulation. C and E, Graphs depict means ± SEM of $Tc_{(80-20\%)}$, the rate at which dopamine was cleared from the synaptic cleft. B–C, At 4 weeks of age, both WT and $En1^{+/-}$ groups showed similar levels of (B) KCl-stimulated dopamine release and (C) synaptic clearance (reuptake) of dopamine. D, KCl-induced releases of dopamine were reduced at positions 1 and 2 of 16-week-old $En1^{+/-}$ mice relative to the WT mice. The maximum amount of dopamine released is presented as mean ± SEM (with significance after unpaired *t*-test: *p < 0.05, **p < 0.01). E, Dopamine reuptake was altered at positions 1 and 2, displaying slower clearance rates in the 16-week $En1^{+/-}$ group and significant differences from WT values (unpaired *t*-test; *p < 0.05, **p < 0.01). *F*, *G*, *H*, HPLC analysis of basal dopamine (*F*), DOPAC (*G*) and HVA (*H*) levels in subregions DM, DL, M and V of 16-week-old WT mice (n = 12–14) and $En1^{+/-}$ mice (n = 10–11). Comparisons were made between $En1^{+/-}$ subregions (unpaired *t*-test: ns = non-significant), and with their respective WT subregion (unpaired *t*-test: *p < 0.05, **p < 0.01, ***p < 0.001, ****p < 0.0001).

$En1^{+/-}$ mice had dramatically reduced dopamine release and reuptake in the dorsal striatum. In the two most dorsal recording positions (positions 1 and 2 in Fig. 6A, left panel), the maximum amplitudes of KCl-evoked dopamine release were reduced by 88% and 53%, respectively, in the $En1^{+/-}$ mice relative to WT (Fig. 6D). Furthermore, in those positions, the $En1^{+/-}$ mice displayed a lower capacity to clear extracellular dopamine, 95% lower at position 1 and 68% lower at position 2 (Fig. 6E).

We next examined whether these results were due to an equivalent regional reduction in local dopamine tissue levels. We measured the tissue levels of dopamine and metabolites in four subregions of the striatum: dorso-medial (DM), dorso-lateral (DL), mid (M) and ventral (V), as shown in Fig. 6A, right panel. At 16 weeks of age, the *En1*$^{+/-}$ mice showed a 26% reduction in the levels of dopamine in the striatum overall. The reduction did not, however, differ significantly between the four subregions of the striatum (Fig. 6F). Thus, the dramatic reduction in dopamine release in the dorsal striatum seen in our in vivo electrochemistry experiments could not be explained by an equivalent regional decrease in tissue levels of dopamine. Similarly, HVA levels in all subregions of the *En1*$^{+/-}$ mice were reduced relative to WT controls, but there were no differences among subregions within the *En1*$^{+/-}$ striatum (Fig. 6H). In contrast, the tissue levels of DOPAC did not significantly differ between the mutant and WT mice for any of the striatal subregions (Fig. 6G). Together, our results suggest that the neurotransmission in the dopaminergic terminals is functionally impaired, specifically in the dorsal striatum of the *En1*$^{+/-}$ mice.

Discussion

We found that early stages of progressive degeneration of nigrostriatal system in the *En1*$^{+/-}$ mice are detectable in the axonal terminals, several weeks before the loss of nigral dopaminergic neurons is evident. In agreement with previous studies (Sonnier et al., 2007), we observed that dopaminergic neurons were not lost during the first 4 postnatal weeks. However, as early as 8 days of age, we identified morphological abnormalities (i.e. swollen axon terminals, so called spheroids) in the nigrostriatal pathway consistent with axonal degeneration. These changes persisted in the oldest mice we studied (32 weeks of age). The abnormal axonal spheroids, at 16 weeks, were immunoreactive for TH, VMAT2, and DAT suggesting that the degenerative process is still at an early stage in the particular neurons that exhibit these axonal changes. Analyses of markers for dopaminergic neurons in striatal tissue samples provide additional evidence for changes occurring in nigrostriatal terminals before the nigral neurons die. Thus, we found that the total striatal levels of TH, dopamine, and DAT were decreased before the number of nigral dopaminergic neurons was substantially reduced in the *En1*$^{+/-}$ mice. Recent reviews on the development of nigrostriatal pathology in PD have emphasized that striatal terminal loss is an early neuropathological event in the disease (Burke and O'Malley, 2013; Cheng et al., 2010). The notion that the pathology starts in the terminal region is supported by a recent study in post-mortem PD brains showing that nigrostriatal neurons exhibit dramatically reduced TH and DAT immunostaining in the striatum as early as within 4–5 years after onset of motor symptoms (Kordower et al., 2013). In contrast, the loss of melanin-containing dopaminergic neurons in the substantia nigra continues during the first decade following PD diagnosis. In short, those post-mortem findings in PD clearly agree with the idea that a loss of function or degeneration of nigrostriatal terminals precedes cell death in the substantia nigra (Kordower et al., 2013).

Earlier literature has proposed that a Wallerian-type axonal degeneration could be a common feature of several progressive neurodegenerative disorders (Coleman and Perry, 2002; Yamamoto and Yue, 2014). Dystrophic axonal spheroids (rich in gamma-synuclein) have been described in the PD hippocampus (Galvin et al., 1999). A recent report suggesting that axonal transport fails in PD brain (Chu et al., 2012), supports the idea that axonal failure is an early feature of PD. Our results using the CLARITY technique in the *En1*$^{+/-}$ mice clearly demonstrate that individual axons in the nigrostriatal pathway undergo fragmentation, which suggests failure of axonal maintenance. Indeed, multiple studies have reported that the En1 protein regulates axon growth and maintenance (Stettler et al., 2012; Wizenmann et al., 2009; Yoon et al., 2012). For example, En1 has been shown to stimulate axon growth and guidance in the retina and tectum by interacting with EphrinA proteins (Brunet et al., 2005; Wizenmann et al., 2009). The proposed molecular mechanism involves the regulation of axonal translation that is activated in the presence of En1 protein. Addition of En1, and its internalization into the axons of cultured retinal ganglion cells, leads to a rapid increase in translation of mitochondrial complex I proteins (Ndufs1, 2, 3) in axons with concomitant increases in ATP levels (Stettler et al., 2012). Another recent study showed that En1 regulates axonal translation of the mRNA of the type V intermediate filament lamin B2. Axonal Lamin B2 promotes mitochondrial function and axonal transport, and reduction in axonal lamin B2 mRNA translation in retinal ganglion cells leads to axonal degeneration (Yoon et al., 2012). Further studies are needed to define if axonal translation and axonal transport are impaired in nigrostriatal dopamine neurons in the *En1*$^{+/-}$ mice.

Mitochondrial dysfunction has been implicated as a major contributor to PD pathogenesis (Exner et al., 2012). Deficiencies in the complex I subunit (both decreased activity and reduced protein levels) have been detected in the PD substantia nigra, linking them to idiopathic PD (Mizuno et al., 1989; Schapira et al., 1989, 1990). The *En1*$^{+/-}$ mouse exhibits decreased levels of mitochondrial proteins in the midbrain. Furthermore, dopamine neurons from the *En1*$^{+/-}$ mice exhibit heightened sensitivity to the neurotoxins 6-hydroxydopamine and MPTP, both of which are suggested to act on mitochondria (Alvarez-Fischer et al., 2011). Consistent with these observations, intracerebral infusions of En proteins result in increased mitochondrial protein translation and are neuroprotective in mitochondrial toxin-based models of PD in vivo (Alvarez-Fischer et al., 2011).

Based on the literature and our own findings, we propose that reduced En1 function initially causes energy failure in dopaminergic terminals. Due to the extensive axonal arborisations, nigrostriatal neurons have been suggested to be particularly susceptible to partial energy failure (Pissadaki and Bolam, 2013). A reduction in energy production, coupled to impaired axonal transport and the accumulation of defective mitochondria requiring clearance by mitophagy, leads to failure of maintenance of dopaminergic axons, finally resulting in their disintegration. The resulting stress on the cell body, as well as a potential reduction of target-derived trophic support (Jackson-Lewis et al., 2000), lead to the eventual death of the neuron.

Recently, the concept that dopaminergic axons might undergo macroautophagy in PD has been discussed extensively (Burke and O'Malley, 2013). Compelling evidence suggests that neurodegeneration in PD involves dysregulation of autophagy, e.g., autophagosomes and protein aggregates have been observed in PD post-mortem brains (Malagelada et al., 2010). Different models show that impaired autophagy in dopaminergic neurons is coupled to aggregation of α-synuclein (Pan et al., 2008), akin to the Lewy aggregates found in dopamine neuron terminals in PD (Deleidi and Maetzler, 2012).

Upon the disrupted maturation of autophagosomes and the subsequent fusion to lysosomes, there is a buildup of immature autophagic vacuoles (Yang et al., 2013). In our ultrastructural analysis, we found that autophagic vacuoles accumulated in the *En1*$^{+/-}$ dopaminergic terminals. The protein LC3B exists in a cytosolic form (LC3-I) and a membrane-bound form (LC3-II), with the latter commonly used as a marker for autophagosomes. The abundance of LC3-II protein is indicative of the number of autophagosomes in a cell (Yamamoto and Yue, 2014). We found that LC3B levels are reduced in the ventral midbrain of the *En1*$^{+/-}$ mice. Furthermore, our immunohistochemical analysis at the cellular level revealed that the soma of the *En1*$^{+/-}$ dopaminergic neurons display a reduction in LC3B-immunoreactive punctae, suggestive of reduced autophagy in these cells. Using our immunohistochemistry protocol, we did not detect LC3B in the dopaminergic terminals in the striatum. However, our ultrastructural observations suggest that autophagic degradation is defective in the nigrostriatal terminals of the *En1*$^{+/-}$ mice.

The mammalian target of rapamycin (mTOR) pathway, which normally acts by inhibiting autophagy mechanisms responsible for degradation and clearance of proteins, has also been directly implicated in PD (Burke and O'Malley, 2013; Laplante and Sabatini, 2012). Inhibition

of mTOR by the administration of rapamycin is neuroprotective in cell- and animal-models of PD (Malagelada et al., 2010). Rapamycin can also increase lysosomal levels in and attenuate death of dopaminergic neurons in another cell culture model of PD (Dehay et al., 2010). In the present study, we observed an up-regulation of pmTOR and its target molecule pS6 inside the dopaminergic neurons of the *En1*$^{+/-}$ mice. This suggests that an imbalance in protein degradation contributes to the degeneration of the nigral *En1*$^{+/-}$ dopaminergic neurons, adding further validity to the *En1*$^{+/-}$ mouse as a PD model.

Our findings suggest that the loss of one *En1* allele causes a functional decline in the subpopulation of dopaminergic neurons that primarily projects into the dorsal striatum. The recent work using a single cell analysis of gene expression has shown that gene expression patterns vary significantly among midbrain dopaminergic neurons in postnatal mice (Poulin et al., 2013). Interestingly, the transcript levels for *En1* and *En2* (which encodes a protein that has some overlapping functions with En1) are lower in the ventral substantia nigra relative to several other dopamine neuron populations in the nigra and ventral tegmental area of the WT mice (Poulin et al., in press). En proteins are not present at similar levels throughout the substantia nigra of adult mice. Whereas En1 expression is widespread throughout the substantia nigra, En2 is only expressed in a subset of nigral neurons. However, En2 transcript level was boosted in the substantia nigra of the *En1*-null mice and seems to compensate for loss of En1 function. To better understand the role of redundancy of En proteins, and selective vulnerability, it will be important to characterize the distribution and expression of En1 and En2 transcripts and proteins in subregions of the substantia nigra of the adult *En1*$^{+/-}$ mice. It is also possible that different subsets of midbrain dopaminergic neurons differ in their dependence on En1. For example, Veenvliet and colleagues have found that in *En1*-null embryos, TH and DAT are decreased in the rostrolateral region of the midbrain but are not altered in the caudal midbrain (Veenvliet et al., 2013). Further studies are needed to define the differential vulnerability of subsets of midbrain dopaminergic neurons to degeneration following reductions of En1 protein and to define whether the most susceptible nigral neurons are analogous to those that degenerate first in PD.

Our results also revealed a striking defect in striatal dopamine neurotransmission in the *En1*$^{+/-}$ mice. In the dorsal striatum of 16-week-old mice (but not 4-week-old mice), we observed a 88% reduction in evoked dopamine release and a 95% reduction in clearance of extracellular dopamine by DAT. Reductions in DAT function are also a feature of early PD, as demonstrated using DAT-SPECT (Kagi et al., 2010). The striatal tissue level of dopamine was also reduced in the *En1*$^{+/-}$ mice at the same age. This reduction was, however, modest (around 26%) and could not explain the severe changes in dopamine neurotransmission that we observed. The overexpression of α-synuclein in PD mouse models suggests that accumulation of α-synuclein impairs dopamine neurotransmission by reducing vesicle load and reducing dopamine release and reuptake (Hansen et al., 2013; Lundblad et al., 2012). We did not observe any obvious α-synuclein accumulation or aggregates in the *En1*$^{+/-}$ mice (data not shown). Thus, α-synuclein accumulation and/or aggregation do not seem to explain the deficits in dopamine neurotransmission in this PD model. Indeed, the *En1* double-null mice reportedly show decreased α-synuclein levels in midbrain dopaminergic neurons, suggesting that En1 normally would enhance α-synuclein levels, possibly as part of a process regulating axon growth (Simon et al., 2001).

En1 protein is required for the specification and maturation of dopaminergic neurons during development (Simon et al., 2001). The observation that the *En1*$^{+/-}$ mouse exhibits a full quota of nigral dopaminergic neurons at birth, and initially displays normal dopamine signaling, excludes dopaminergic loss due to a developmental effect. In concordance with other proteins (e.g. Pitx3 and Nurr1) that govern dopaminergic neuron development together with En1, the expression of En1 continues during adulthood (Simon et al., 2001) and is required for the maintenance of axonal integrity and dopaminergic neuron survival. Interestingly, mutations in the Nurr1 and Pitx3 genes also associate to PD (Fuchs et al., 2009; Le et al., 2003). Similarly to the *En1*$^{+/-}$ mice, conditional knockout mice where Nurr1 is ablated in dopaminergic neurons during adulthood exhibit progressive dopaminergic neuron pathology, show progressive development of TH-positive dystrophic dendrites, and reduction of striatal dopamine (Decressac et al., 2012; Kadkhodaei et al., 2013).

In conclusion, we report that the loss of En1 function in the mice causes axonal degeneration that precedes dopamine cell death. Several features we have observed suggest that the nigrostriatal axons die back slowly, causing eventual nigral cell death in a process involving autophagy. An important additional characteristic of our mouse model is severe impairment in dopamine neurotransmission in the dorsal striatum. The protracted course of axonal degeneration and nigral cell death in the *En1*$^{+/-}$ mouse already makes it very suitable for studies on potential neuroprotective agents. In the future, it will be useful to explore how the degeneration of the nigrostriatal pathway in the *En1*$^{+/-}$ mice responds to situations when α-synuclein levels are elevated experimentally.

Materials and methods

Animals

The mice were treated in accordance with the Guide for the Care and Use of Laboratory animals (US National Institutes of Health) and with approval of the Van Andel Research Institute's IACUC. The *En1* heterozygous mice were generated as described earlier and were maintained on an OF1 genetic background (Sonnier et al., 2007). They express the *LacZ* gene downstream of the *En1* promoter, which drives the expression of β-galactosidase (β-gal). The mutant *TH–GFP* mice were also generated as described above and maintained on a C57BL-6J genetic background (Sawamoto et al., 2001). The *TH–GFP* mutant mice were backcrossed at least eight generations to OF1 mice, before being crossed with the *En1*$^{+/-}$ mice to generate the double mutant *TH–GFP*; *En1*$^{+/-}$ animals.

Immunohistochemistry (IHC)/immunofluorescence (IF)

The mice were anesthetized with pentobarbital and perfused intracardially with 4% paraformaldehyde (PFA). Intact brains were removed and post-fixed overnight in the PFA solution before being equilibrated in 30% sucrose. Brains were serially (6) sectioned into 30- to 40-μm-thick coronal and sagittal sections for IF and IHC.

For TH IHC, free-floating sections were washed with 0.1 M PBS (pH 7.4), incubated with 3% H_2O_2 for 10 min to quench endogenous peroxidase activity, and were blocked for 1 h with 10% normal goat serum and 0.25% Triton X-100. Next, the sections were incubated overnight at 4 °C with the TH primary antibody (1:1500, Pel-freez Biologicals, USA). The next day, the sections were washed with 0.1% Triton X in PBS and incubated with a biotinylated goat anti-rabbit secondary antibody (1:500, Vector Laboratories, USA) for 1 h at room temperature. The intensity signal was then amplified by incubating the sections with the Avidin/Biotin ABC reagent (Vector Laboratories, USA). Finally, the immunostaining was revealed by incubation with the chromogen diaminobenzidine (DAB), producing a brown color visible in bright-field light microscopy. Sections were dehydrated in increasing ethanol concentrations, cleared in xylene, and mounted on slides using DPX medium (Electron Microscopy Sciences, USA).

For double-labeling IF, the H_2O_2 quenching step was omitted and the sections were directly blocked with normal goat serum before incubation overnight at 4 °C with the following primary antibodies: TH (1:1500, Pel-freez Biologicals, USA); GFP (1:500, Abcam, USA); β-gal (1:500, Abcam, USA); TH (1:1500, Chemicon, USA); p-mTOR (1:200, Cell signaling, USA); p-S6 (1:400, Cell signaling, USA); LC3B (1:500, Cell signaling, USA) or En1/2 (1:1000, produced in Alain Prochiantz's laboratory). The secondary antibodies goat anti-rabbit and goat anti-mouse coupled to Alexa 488 or 594 (1:500, Jackson ImmunoResearch,

USA) were used. Nuclei were stained by DAPI (Sigma, USA). The sections were mounted with ProLong Gold antifade medium (Life Technologies, USA) and coverslipped. Sections were viewed under a NIKON eclipse Ni-U fluorescence microscope (Nikon, USA); images were captured with a Retiga Exi digital camera using NIS Elements AR 4.00.08 software (Nikon, USA). Confocal imaging was performed with a Nikon Eclipse Ti-E inverted microscope (Nikon, USA), followed by deconvolution techniques using Huygens software (Scientific Volume Imaging, USA).

Measurement of fluorescence intensity and densitometry

A total of two sections per brain containing the substantia nigra region and three mice per group were stained with antibodies directed against TH, pmTOR, pS6, and LC3B as mentioned above. After immunofluorescence or histochemical staining, four 40× images were taken from each section and the mean intensity of fluorescence of pmTOR, pS6, LC3B, and TH in TH-positive neurons, as well as counting of LC3B immunoreactive punctae in TH-positive neurons in substantia nigra were quantified using NIS Elements AR 4.00.08 software (Nikon, USA).

CLARITY

Thirty-two-week-old WT and *En1*$^{+/-}$ mice were perfused with hydrogel monomers solution, as described earlier (Chung et al., 2013). The brains were extracted and stored in the hydrogel monomers solution for 3 days at 4 °C, followed by hydrogel tissue embedding at 37 °C for 3 h. The brain hemispheres were separated and processed individually. The samples were incubated in a clearing solution (which contained sodium borate buffer [200 mM (pH 8.5) and 4% SDS]), at 37 °C with gentle rotation for 5–6 weeks. Once the samples were clarified, they were washed for 2 days with PBS plus 0.1% Triton X (PBS-T).

For TH immunostaining, clarified brain samples were incubated at 37 °C with gentle rotation for one week with the primary antibody (1:50, Calbiochem, USA) diluted in PBS-T, followed by 3 days of washes with PBS-T at 37 °C. The samples were then incubated with the secondary antibody, goat anti-rabbit coupled to Alexa 594 (1:200, Jackson ImmunoResearch, USA) diluted in PBS-T, at 37 °C for one week; then they were washed with PBST at 37 °C for 3 days. Before confocal imaging, samples were mounted on coverglass-bottomed dishes (Willco) with FocusClear (CelExplorer) and allowed to equilibrate overnight at room temperature. The clarified samples were then imaged using an inverted Nikon A1-RSi confocal microscope with a 10X, 0.3 NA air objective and a 20×, 0.75 NA multi-immersion objective with 85% glycerol lens immersion. Image stacks were acquired with a Z-step spacing of 0.85 μm. The lateral and axial imaging resolution was determined by a Nyquist sampling calculator, and all images were deconvolved using Huygens Pro (Scientific Volume Imaging, Netherlands).

Stereological estimation of dopaminergic neurons in the substantia nigra

The dopaminergic neurons of the WT and *En1*$^{+/-}$ mice were identified after TH DAB staining of midbrain regions with a 2× objective and the substantia nigra region was outlined based on the Allen mouse brain atlas. Quantitative estimation of TH-positive neurons was performed in every 6th section of the substantia nigra. Briefly, the unbiased sampling and blinded stereological counting were done using the optical fractionator probe in Stereo Investigator software (MBF Bioscience, USA). The parameters used include a 60× oil objective, a counting frame size of 60 × 60, a sampling site of 100 × 100, a dissector height of 12 μm, 2 μm guard zones and the Schmitz-Hof's second estimated coefficient error less than 0.1. A total of 6 to 7 animals per group were used and 5 to 8 sections per animal were counted.

Quantification of the TH-positive dystrophic terminals

After TH immunostaining of 40-μm-thick striatal sections, one section per mouse (n = 4–5 animals per group) at position bregma 0.7–0.9 mm (Paxinos mouse atlas) was imaged with a 40× objective covering in average 10 fields of view in the striatum. Automated counting of degenerating profiles was performed using the Image J plugin "Analyze particles" for a total of 38–45 sampling sites of 375 μm × 375 μm in size. For morphological criteria of insertion, positive dystrophic terminals were thresholded for a minimum size of 3 μm^2 and a circularity index of >0.8. By setting the parameters, we ensured that segmented degenerating profiles were counted without counting axons or dendrites.

In vivo electrochemistry

Highspeed chronoamperometric recordings were made using FAST-16mkII software and hardware (Quanteon, L.L.C. Nicholasville, KY, USA) fitted with carbon fiber electrodes (fiber diameter 30 μm; exposed length 120–150 μm, type SPF1a, Quanteon, USA) as previously described in (Lundblad et al., 2012). In short, a square wave potential was applied (+0.55 V; resting 0.0 V vs. Ag/AgCl reference) and the resulting oxidation and subsequent reduction currents collected by the carbon fiber electrodes were integrated during the final 80% of each 100-ms pulse. Oxidation and reduction currents were continually recorded and integrated over 0.5 s (2 Hz recording). Electrodes were then dried in dry oven at 200 °C, dipped 1 s in 5% Nafion (Sigma, Sweden), and placed back in oven at 200 °C for 5 min. This procedure was repeated three times. Nafion coating was used to prevent detection of anionic substances and thus increase the sensitivity for dopamine. Each electrode was calibrated individually against fixed 2 μM increments of dopamine in 0.1 M PBS solution (pH 7.4) at room temperature. Selectivity against ascorbic acid was determined as the ratio of oxidation current response to ascorbic acid and dopamine. Limit of detection was less than 47 nM for all electrodes used, linearity of response was r2 > 0.998 and selectivity was greater than 339:1 for dopamine against ascorbic acid.

Each electrode was fitted with a glass capillary (outer diameter 20–25 μm) connected to a micropressure system (Parker Picospritzer III, Aldax, Sweden) for local application of 100–120 nl KCl (120 mM). The distance between the tip of the electrode and the tip of the glass capillary was set to 90–110 μm and the ejected KCl volume was determined by movement of the meniscus in the glass capillary and measured using a stereo microscope fitted with a reticule. An Ag/AgCl electrode used as a reference electrode in vivo was prepared by electroplating a Ag wire in 1 M HCl solution saturated with NaCl for at least 30 min.

Recordings were made bilaterally from striatum from all animals at the coordinates AP: +0.5 mm; L: ±2.0 at 6 different depths. To enable measurement from the most dorsal part of striatum, KCl was ejected at −1.5 mm DV coordinate and moved down 250 μm until dopamine release (peak amplitude >0.2 μM) was obtained. The first dopamine release depth (peak amplitude >0.3 μM) was considered the first in the series of 6 depth coordinates. From the first coordinate in the striatum the electrode was lowered in three 250-μm increments and then two increments of 500 μm.

Recordings were made at 4 or 16 weeks of age for the WT and *En1*$^{+/-}$ mice. The animals were anesthetized using isoflurane anesthesia (4% in induction chamber, 1.5% in the stereotaxic frame throughout the recording session) and positioned in a stereotaxic frame. Body temperature was maintained at 37 °C with a constant temperature heating pad connected to a thermostatically controlled water pump (Micro-Temp LT, USA). The skull and dura were removed bilaterally above the recording sites. The electrode/glass capillary assembly was lowered into the brain to the first recording coordinate using a micromanipulator (Narishige MO-10, Japan) and left for at least 30 min to provide a baseline. A fixed volume of KCl (100 nl ± 10 nl) was ejected at each recording position. Data from the two hemispheres were averaged on each recording point. Due to technical

issues, for five animals, data is available from only one of the two hemispheres (*En1*$^{+/-}$ 4-week group: 3 animals; WT 16-week group: 2 animals).

All parameters of the amperometric data were calculated using FAST analysis version 4.0 for Mac (Quanteon LLC, USA). Peak amplitude was calculated as the difference of (maximum dopamine concentration after KCl injection)–(baseline prior to KCl injection). Clearance (Tc) is defined as the linear rate of concentration decrease (μM/s) between T_{60} (time when signal amplitude is 60% of peak amplitude) and T_{40} (time when signal amplitude is 40% of peak amplitude).

Immunoblots

The animals were euthanized by rapid decapitation, and brains were then quickly removed and dissected to collect striata and substantia nigra regions. The tissues were stored at −80 °C until use. Total proteins were extracted in RIPA buffer supplemented with protease inhibitor cocktail (Sigma, USA), phosphatase inhibitors (3 mM sodium pyrophosphate, 10 mM sodium fluoride, 2 mM sodium orthovanadate), and 1 mM PMSF. The lysates were centrifuged at 15 000 × *g* for 20 min at 4 °C and the supernatants were used in immunoblotting. After protein quantitation (BCA assay kit, Pierce, USA), proteins were separated by SDS-PAGE using 4–15% gradient gels (Biorad, USA) and transferred to nitrocellulose membrane. Blots were blocked with 5% dry milk diluted in 0.1 M TBS/0.1% Tween-20 and were incubated overnight at 4 °C, with primary antibodies [TH, 1:1500, Pel Freez Biologicals, USA; DAT, 1:1000; pmTOR (Ser2448), 1:1000; mTOR, 1:1000; pS6 ribosomal protein (Ser235/236), 1:1000; S6 ribosomal protein, 1:2000; LC3B, 1:1000, Cell Signaling, USA] diluted in a solution of 0.1 M TBS, 0.1% Tween-20, 5% BSA. Incubations with secondary antibodies goat-anti-rabbit IgG (H&L) IRDye® 800 Conjugated (1:10000, Rockland, USA) and Alexa Fluor 680 goat anti-mouse IgG (H + L) (1:10000, Invitrogen, USA) were performed in blocking solution for 1 h at room temperature. Band detection was performed using the Licor Odyssey system and quantified using Image J software. Later, blots were stripped with the Restore Western Blot Stripping Buffer (Thermo Scientific, USA) and reblotted for β-Actin (1:10000, Abcam, USA).

Transmission electron microscopy

The mice were perfused with 2.5% glutaraldehyde/4% PFA in 0.1 M sodium cacodylate buffer. Using a vibratome, 1-mm^3 blocks were cut from the dorsal lateral striatum and post-fixed for at least 24 h. The tissues were then processed through various treatments that revealed contrast between cellular compartments. The sections were first incubated in more specialized fixative solutions. They were then post-fixed in 0.1% tannic acid for 1 h at room temperature. After washes with 0.1 M cacodylate buffer, the samples were incubated with the second post-fixative solution containing osmium tetroxide and potassium ferrocyanide at room temperature for 2 h. Then, the samples were ready to be stained and were first treated for 30 min with a solution of thiocarbohydrazide, which deposited an opaque layer of electrons to increase membrane contrast. The second staining step was incubation with 2% osmium tetroxide for 60 min at room temperature, which also increased contrast of extracellular compartments.

Next, sections were incubated overnight at 4 °C with the primary stain solution of 1% uranyl acetate, a heavy metal salt that stains nucleic acids and proteins. After washing with water, the sections were incubated with the secondary stain, lead aspartate, to increase intracellular contrast. Next, the sections went through a series of incubation steps of increasing ethanol concentrations (50, 75, 85, 95, 100%), followed by a final wash with propylene oxide. The samples were embedded with the Epon resin (following the manufacturer's instructions; EMbed-812 embedding kit, Electron Microscopy Sciences, USA) and propylene oxide at a ratio of 1:1 overnight at room temperature. The following day, the sections were transferred to fresh concentrated epon solution and incubated for 90 min. The last steps of the staining process consist of mounting of the sections in a mold full with epon and curing at 60 °C for 48 h.

Serial blockface images (80 nm thick slices) were obtained with a Zeiss Sigma VP scanning electron microscope equipped with a Gatan 3View in-chamber ultramicrotome, at a resolution of 5 nm per pixel. The analysis of the images and annotation were performed with ImageJ.

HPLC

Extracellular dopamine and its metabolites were measured by our previously published HPLC technique (Spieles-Engemann et al., 2010) on either the entire striatum tissue (caudate and putamen regions) or on micropunches from different striatal subregions. The micropunches were dissected from the tissue at a 1-mm diameter. Next, the samples to analyze were homogenized in an antioxidant buffer (0.4 N perchlorate, 1.343 mM EDTA and 0.526 mM sodium metabisulfite). After centrifugation, a fraction of the supernatants containing the cytoplasmic proteins was run on the HPLC machine, while another fraction was used to assess protein concentration. A Microsorb MV C-18 column (5 Am, 4.6_250 mm, Varian, Walnut Creek, CA) was used to separate the neurotransmitter from its metabolites, which were detected using a 12-channel coulometric array detector (CoulArray 5200, ESA, Chelmsford, MA) attached to a Waters 2695 Solvent Delivery System (Waters, Milford, MA) under the following conditions: flow rate of 1 ml/min; detection potentials of 50, 175, 350, 400 and 525 mV; and scrubbing potential of 650 mV. The mobile phase was 10% methanol containing 21 g/L (0.1 M) citric acid, 10.65 g/L (0.075 M) Na_2HPO_4, 176 mg/L (0.8 M) heptanesulfonic acid, and 36 mg/L (0.097 mM) EDTA at a pH of 4.1. Dopamine, DOPAC, and HVA levels were normalized to the amounts of proteins and reported as “ng/mg protein”.

Statistical analysis

Statistical analyses were calculated using GraphPad Prism, version 6.0d. For comparisons between the WT and *En1*$^{+/-}$ groups for immunoblot band intensities, stereological counting, fluorescence intensity, and HPLC data analyses, p values were determined after statistical unpaired *t*-tests were performed, followed by Welch's correction. For establishing the effects of genotype and anatomical region on in vivo electrochemistry and HPLC data from striatal punches, as well as genotype and age effects on stereological quantitation of TH-positive neurons, protein levels of TH and DAT, and counting of axonal swellings, we performed two-factor ANOVA analyses, followed by Tukey's multiple comparison tests.

Supplementary data to this article can be found online at http://dx.doi.org/10.1016/j.nbd.2014.09.012.

Acknowledgments

We acknowledge the excellent technical assistance provided by Alicia Flasch, Birgit Haraldsson, Darcy Kaufman, Britt-Marie Lindberg, Marie Persson Vejgården and Allyson Cole-Strauss. Furthermore, we are also grateful to Peter Ekström for the cell imaging assistance. We thank Olivia Beaudoin for her help in designing some experiments and Bruno Saubaméa and Virginie Mignon of the Cellular and Molecular Imaging Platform, CRP2 - UMS 3612 CNRS - US25 INSERM-IRD - Université Paris Descartes for their help with immunohistology. This work was supported by the Van Andel Research Institute, The Swedish Research Council, The Strong Research Environment Multipark (Multidisciplinary research in Parkinson's disease at Lund University), The Swedish Parkinson Foundation (Parkinsonfonden), Konung Gustav V:s och Drottning Victorias Stiftelse, Thorsten och Elsa Segerfalks Stiftelse, Magnus Bergvalls stiftelse, Crafoordska stiftelsen and Åke Wibergs Stiftelse, The Campbell Foundation, The Morris K. Udall Center of Excellence in Parkinson's Disease Research at Michigan State University (P50-NS058830), Secchia

Family Foundation, Collège de France, Centre National de la Recherche Scientifique (CNRS) and Institut National de la Santé et de la Recherche Médicale (INSERM), Global Research Laboratory Program (2009-00424), Agence Nationale pour la Recherche (ANR-11-BLAN-069467) and the European Research Council (advanced grant no 339379).

References

Alvarez-Fischer, D., et al., 2011. Engrailed protects mouse midbrain dopaminergic neurons against mitochondrial complex I insults. Nat. Neurosci. 14, 1260–1266.
Bezard, E., et al., 2013. Animal models of Parkinson's disease: limits and relevance to neuroprotection studies. Mov. Disord. 28, 61–70.
Blesa, J., et al., 2012. Classic and new animal models of Parkinson's disease. J. Biomed. Biotechnol. 2012, 845618.
Brunet, I., et al., 2005. The transcription factor Engrailed-2 guides retinal axons. Nature 438, 94–98.
Burke, R.E., O'Malley, K., 2013. Axon degeneration in Parkinson's disease. Exp. Neurol. 246, 72–83.
Cheng, H.C., et al., 2010. Clinical progression in Parkinson's disease and the neurobiology of axons. Ann. Neurol. 67, 715–725.
Chu, Y., et al., 2012. Alterations in axonal transport motor proteins in sporadic and experimental Parkinson's disease. Brain 135, 2058–2073.
Chung, K., et al., 2013. Structural and molecular interrogation of intact biological systems. Nature 497, 332–337.
Coleman, M.P., Perry, V.H., 2002. Axon pathology in neurological disease: a neglected therapeutic target. Trends Neurosci. 25, 532–537.
Decressac, M., et al., 2012. alpha-Synuclein-induced down-regulation of Nurr1 disrupts GDNF signaling in nigral dopamine neurons. Sci. Transl. Med. 4, 163ra156.
Dehay, B., et al., 2010. Pathogenic lysosomal depletion in Parkinson's disease. J. Neurosci. 30, 12535–12544.
Deleidi, M., Maetzler, W., 2012. Protein clearance mechanisms of alpha-synuclein and amyloid-Beta in Lewy body disorders. Int. J. Alzheimers Dis. 391438.
Exner, N., et al., 2012. Mitochondrial dysfunction in Parkinson's disease: molecular mechanisms and pathophysiological consequences. EMBO J. 31, 3038–3062.
Fuchs, J., et al., 2009. The transcription factor PITX3 is associated with sporadic Parkinson's disease. Neurobiol. Aging 30, 731–738.
Galvin, J.E., et al., 1999. Axon pathology in Parkinson's disease and Lewy body dementia hippocampus contains alpha-, beta-, and gamma-synuclein. Proc. Natl. Acad. Sci. U. S. A. 96, 13450–13455.
Hansen, C., et al., 2013. A novel alpha-synuclein-GFP mouse model displays progressive motor impairment, olfactory dysfunction and accumulation of alpha-synuclein-GFP. Neurobiol. Dis. 56, 145–155.
Jackson-Lewis, V., et al., 2000. Developmental cell death in dopaminergic neurons of the substantia nigra of mice. J. Comp. Neurol. 424, 476–488.
Kadkhodaei, B., et al., 2013. Transcription factor Nurr1 maintains fiber integrity and nuclear-encoded mitochondrial gene expression in dopamine neurons. Proc. Natl. Acad. Sci. U. S. A. 110, 2360–2365.
Kagi, G., et al., 2010. The role of DAT-SPECT in movement disorders. J. Neurol. Neurosurg. Psychiatry 81, 5–12.
Kordower, J.H., et al., 2013. Disease duration and the integrity of the nigrostriatal system in Parkinson's disease. Brain 136, 2419–2431.
Laplante, M., Sabatini, D.M., 2012. mTOR signaling in growth control and disease. Cell 149, 274–293.
Le Pen, G., et al., 2008. Progressive loss of dopaminergic neurons in the ventral midbrain of adult mice heterozygote for Engrailed1: a new genetic model for Parkinson's disease? Parkinsonism Relat. Disord. 14 (Suppl. 2), S107–S111.
Le, W.D., et al., 2003. Mutations in NR4A2 associated with familial Parkinson disease. Nat. Genet. 33, 85–89.
Lundblad, M., et al., 2012. Impaired neurotransmission caused by overexpression of alpha-synuclein in nigral dopamine neurons. Proc. Natl. Acad. Sci. U. S. A. 109, 3213–3219.
Malagelada, C., et al., 2010. Rapamycin protects against neuron death in in vitro and in vivo models of Parkinson's disease. J. Neurosci. 30, 1166–1175.
Mizuno, Y., et al., 1989. Deficiencies in complex I subunits of the respiratory chain in Parkinson's disease. Biochem. Biophys. Res. Commun. 163, 1450–1455.
Pan, T., et al., 2008. The role of autophagy–lysosome pathway in neurodegeneration associated with Parkinson's disease. Brain 131, 1969–1978.
Pickel, V.M., et al., 1981. Ultrastructural immunocytochemical localization of tyrosine hydroxylase in the neostriatum. Brain Res. 225, 373–385.
Pissadaki, E.K., Bolam, J.P., 2013. The energy cost of action potential propagation in dopamine neurons: clues to susceptibility in Parkinson's disease. Front. Comput. Neurosci. 7, 13.
Poulin, J.-F., Drouin-Ouellet, J., Cicchetti, F., Awatramani, R.B., 2013. High throughput single-cell expression analysis of midbrain dopamine neurons reveals Aldh1a1 as marker of vulnerability in a model of Parkinson's disease. Program No. 46.08. 2013 Neuroscience Meeting Planner. Society for Neuroscience, San Diego, CA, 2013. Online.
Poulin, J.-F., et al., 2014. Defining midbrain dopaminergic neuron diversity by single-cell gene profiling. Cell Rep. (in press).
Sanchez-Perez, A.M., et al., 2012. Parkinson's disease and autophagy. Park. Dis. 429524.
Sawamoto, K., et al., 2001. Visualization, direct isolation, and transplantation of midbrain dopaminergic neurons. Proc. Natl. Acad. Sci. U. S. A. 98, 6423–6428.
Schapira, A.H., 2011. Mitochondrial pathology in Parkinson's disease. Mt Sinai J. Med. 78, 872–881.
Schapira, A.H., et al., 1989. Mitochondrial complex I deficiency in Parkinson's disease. Lancet 1, 1269.
Schapira, A.H., et al., 1990. Mitochondrial complex I deficiency in Parkinson's disease. J. Neurochem. 54, 823–827.
Simon, H.H., et al., 2001. Fate of midbrain dopaminergic neurons controlled by the engrailed genes. J. Neurosci. 21, 3126–3134.
Son, J.H., et al., 2012. Neuronal autophagy and neurodegenerative diseases. Exp. Mol. Med. 44, 89–98.
Sonnier, L., et al., 2007. Progressive loss of dopaminergic neurons in the ventral midbrain of adult mice heterozygote for Engrailed1. J. Neurosci. 27, 1063–1071.
Spieles-Engemann, A.L., et al., 2010. Stimulation of the rat subthalamic nucleus is neuroprotective following significant nigral dopamine neuron loss. Neurobiol. Dis. 39, 105–115.
Stettler, O., et al., 2012. Engrailed homeoprotein recruits the adenosine A1 receptor to potentiate ephrin A5 function in retinal growth cones. Development 139, 215–224.
Veenvliet, J.V., et al., 2013. Specification of dopaminergic subsets involves interplay of En1 and Pitx3. Development 140, 3373–3384.
Wizenmann, A., et al., 2009. Extracellular Engrailed participates in the topographic guidance of retinal axons in vivo. Neuron 64, 355–366.
Wurst, W., et al., 1994. Multiple developmental defects in Engrailed-1 mutant mice: an early mid-hindbrain deletion and patterning defects in forelimbs and sternum. Development 120, 2065–2075.
Yamamoto, A., Yue, Z., 2014. Autophagy and its normal and pathogenic States in the brain. Annu. Rev. Neurosci. 37, 55–78.
Yang, Y., et al., 2013. Autophagy in axonal and dendritic degeneration. Trends Neurosci. 36, 418–428.
Yoon, B.C., et al., 2012. Local translation of extranuclear lamin B promotes axon maintenance. Cell 148, 752–764.